

Tunable Phonon-Driven Magnon Spin Currents in Altermagnets

Sofie Helene Ursin,¹ Mathias Kläui,^{2,3} and Kjetil M. D. Hals¹

¹Department of Engineering Sciences, University of Agder, 4879 Grimstad, Norway

²Institute of Physics, Johannes Gutenberg University Mainz, Staudingerweg 7, 55128 Mainz, Germany

³Center for Quantum Spintronics, Department of Physics, Norwegian University of Science and Technology, 7491 Trondheim, Norway

(Dated: May 20, 2026)

Altermagnets have recently attracted considerable interest due to their unique symmetry-governed spintronic properties. Here, we investigate phonon-induced magnon spin currents in a two-dimensional altermagnet. Starting from a microscopic theory of the coupled magnon-phonon system, we derive the nonequilibrium magnon distribution generated by selective phonon excitations. We show that the resulting spin currents exhibit a pronounced *d*-wave symmetry with respect to the phonon momentum. Moreover, the spin current along the altermagnetic directions can be completely reversed by tuning the phonon frequency. These findings establish altermagnets as promising platforms for realizing highly tunable, phonon-driven coherent terahertz magnon spin currents.

Altermagnetism has recently emerged as a novel class of antiferromagnetically ordered spin systems in which crystal symmetry, in combination with exchange coupling, lifts the spin degeneracy of the electronic band structure [1, 2]. Recent angle-resolved photoemission spectroscopy experiments have revealed pronounced band splitting, with the spin polarization of the electronic bands exhibiting *g*-wave [3–12] and *d*-wave [13, 14] symmetries in momentum space — a key hallmark of altermagnetism. This mechanism enables efficient spin-current generation without requiring net magnetization or strong spin-orbit coupling (SOC), while preserving the key advantages of antiferromagnets for spintronic applications [15], including the absence of stray fields and ultrafast terahertz (THz) spin dynamics. In addition, altermagnets host a variety of distinctive symmetry-governed phenomena, such as anomalous transport effects [16–25] without net magnetization, unconventional optical responses [26, 27], and spin-splitter torques [28–30].

The distinctive symmetry of altermagnets also manifests in their collective spin excitations [31–34]. The magnon spectrum exhibits a momentum-dependent chiral band splitting, with degeneracies remaining only on a symmetry-governed submanifold. Furthermore, the chiral splitting displays an alternating symmetry across the Brillouin zone. This behavior contrasts sharply with conventional antiferromagnets, where the magnon modes are typically doubly degenerate in the absence of external magnetic fields or other symmetry breaking [35]. Recent inelastic neutron scattering experiments have directly observed this chiral splitting in altermagnets [36, 37].

The two nondegenerate chiral magnon branches in altermagnets carry opposite spin angular momentum, enabling magnon spin currents along altermagnetic directions without external magnetic fields. The resulting spin-current polarization is expected to show an alternating symmetry in the Brillouin zone, consistent with the chiral splitting. Experimental signatures of this alternating symmetry were recently observed by applying

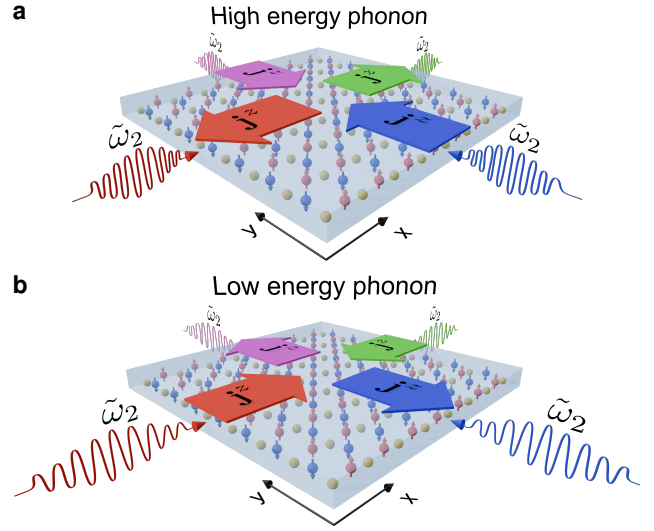


FIG. 1. Visualization of the complete reversal of the magnon spin current \mathbf{j}^z along the altermagnetic directions induced by tuning the phonon frequency $\tilde{\omega}_2(\mathbf{q})$. The colors associate selective phonon excitations with the resulting spin-current directions. (a) Spin currents generated by high-energy phonons. (b) Spin currents generated by low-energy phonons.

a temperature gradient along different crystallographic directions in the *d*-wave altermagnet LuFeO_3 [24].

An essential ingredient for understanding the generation and control of magnon spin currents is their coupling to the phonons of the underlying lattice. In altermagnets, this coupling is expected to play a particularly important role. First, phonons couple differently to the two spin sublattices as the anisotropic exchange interaction give rise to different coupling strengths between phonons and the two magnon branches. Second, the band splitting along the altermagnetic directions leads to a momentum-dependent imbalance in the excitation of the two magnon branches. Despite its fundamental importance, the interplay between magnons and phonons in

altermagnets has thus far received limited attention [38], and its consequences for magnon spin-current transport remain largely unexplored.

Here, we investigate the excitation of magnons by phonons in an altermagnetic Lieb lattice. By developing a microscopic theory of the coupled magnon–phonon system, we perturbatively compute—within the Keldysh formalism—the nonequilibrium magnon spin current induced by single phonon modes. Remarkably, we find that the polarization of the generated spin current can be tuned via both the phonon frequency and momentum. For a fixed frequency, the spin-current polarization for different phonon propagation directions reflects the alternating symmetry of the chiral magnon band splitting. However, the overall sign of the spin current can be reversed by tuning the phonon frequency. Both the alternating symmetry and the frequency dependence of the spin current vanish in the absence of altermagnetic exchange coupling, identifying these effects as clear symmetry-governed signatures of altermagnetism.

We consider a monolayer Lieb lattice with point group symmetry D_{4h} [39], grown on a substrate [40]. The substrate breaks both inversion and the horizontal mirror symmetry, lowering the point group to C_{4v} . The resulting space group is the symmorphic group $P4mm$ and the corresponding magnetic point group contains the elements [32]: $(E|0)$, $(C_{2z}|0)$, $(\sigma_x|0)$, $(\sigma_y|0)$, $(C_{4z}^+|\mathcal{T})$, $(C_{4z}^-|\mathcal{T})$, $(\sigma_{xy}|\mathcal{T})$, $(\sigma_{x\bar{y}}|\mathcal{T})$. Here, the operators on the left act on real space and the time-reversal operator \mathcal{T} flips the spins. The symmetry operations C_{2z} and C_{4z}^+ (C_{4z}^-) denote a twofold counterclockwise rotation and a fourfold counterclockwise (clockwise) rotation about the z axis, respectively. σ_x , σ_y , σ_{xy} , $\sigma_{x\bar{y}}$ correspond to reflections with respect to the xz , yz , and the diagonal planes.

In the following, we investigate the nonequilibrium magnon spin current induced by selective phonon excitations. To this end, we first develop a theory for the phonons. Since our primary interest is the impact of individual phonon modes on the magnons, we treat a given mode as classically coherent in its coupling to the magnons. Motivated by laser-driven excitations, we focus on the optical phonon modes. To obtain analytic expressions for the phonon eigenvalues and eigenvectors, we restrict the analysis to nearest-neighbor interactions.

The phonon spectrum is determined by the eigenvalue problem [41]

$$\mathbf{D}(\mathbf{q}) \cdot \mathbf{e}_n(\mathbf{q}) = \tilde{\omega}_n^2(\mathbf{q}) \mathbf{e}_n(\mathbf{q}), \quad (1)$$

where

$$\mathbf{D}(\mathbf{q}) = \begin{pmatrix} \mathbf{D}_{11} & \mathbf{D}_{12} & \mathbf{D}_{13} \\ \mathbf{D}_{21} & \mathbf{D}_{22} & \mathbf{D}_{23} \\ \mathbf{D}_{31} & \mathbf{D}_{32} & \mathbf{D}_{33} \end{pmatrix}, \quad \mathbf{e}_n(\mathbf{q}) = \begin{pmatrix} \mathbf{e}_n(1|\mathbf{q}) \\ \mathbf{e}_n(2|\mathbf{q}) \\ \mathbf{e}_n(3|\mathbf{q}) \end{pmatrix}, \quad (2)$$

are the dynamical matrix and eigenvectors, respectively. Here, $\mathbf{D}_{kk'}$ is a 3×3 matrix with elements $D_{kk'}^{\alpha\beta}$ describ-

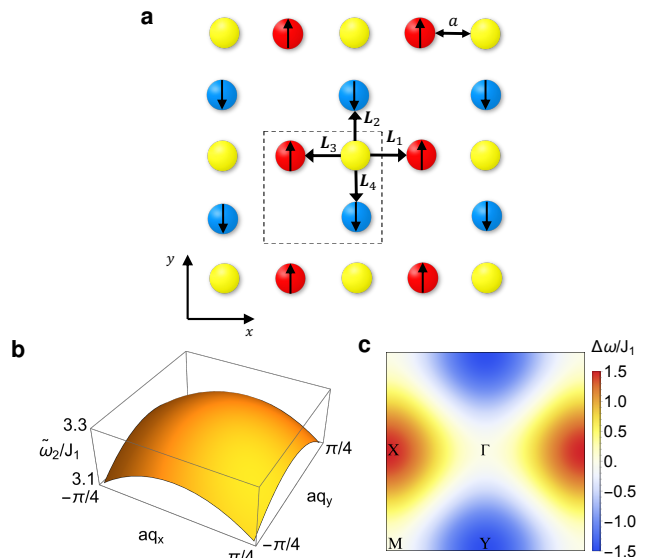


FIG. 2. (a) A monolayer altermagnetic Lieb lattice. The unit cell contains three atoms: a spin-up, a spin-down, and a nonmagnetic atom. The four nearest-neighbor bonds connect each spin atom to the nonmagnetic atom, while no direct coupling occurs between the spin atoms. (b) Phonon mode $\tilde{\omega}_2(\mathbf{q}) = \omega_0^{(2)} \sqrt{1 - a^2(q_x^2 + q_y^2)}/8$ with $\omega_0^{(2)} = 1.3\omega_0$ where $\omega_0 = 4S\sqrt{K_z^2 - 4J_1K_z}$. (c) The magnon band-splitting $\Delta\omega(\mathbf{k})$ in Eq. (9). In (b)-(c), we use $J_1 = 25.7$ meV, $K_z/J_1 = -0.1$, $J_2/J_1 = -0.4$, $\Delta J_2/J_1 = -0.2$, and $\hbar = S = 1$.

ing the interaction between atom k and k' in the unit cell. $\mathbf{e}_n(k|\mathbf{q}) = [e_{n,x}(k|\mathbf{q}), e_{n,y}(k|\mathbf{q}), e_{n,z}(k|\mathbf{q})]^T$ is the part of the eigenvector corresponding to atom k in the unit cell and $\tilde{\omega}_n(\mathbf{q})$ is the frequency of phonon mode n with momentum \mathbf{q} . We further label atom 1 as spin-up, 2 as spin-down and 3 as the non-magnetic atom in the unit cell. Restricting to nearest-neighbor interactions, we obtain $\mathbf{D}_{12} = \mathbf{D}_{21} = \mathbf{0}$, since the spin atoms are not directly coupled. The remaining elements $\mathbf{D}_{kk'}$ are given by [41]

$$D_{kk'}^{\alpha\beta}(\mathbf{q}) = \frac{1}{\sqrt{m_k m_{k'}}} \sum_{l, l'} \Phi_{\alpha\beta} \begin{pmatrix} l & l' \\ k & k' \end{pmatrix} e^{i\mathbf{q} \cdot [\mathbf{r}(l') - \mathbf{r}(l)]}, \quad (3)$$

where m_k and $m_{k'}$ denote the atomic masses of sublattices k and k' , respectively. The indices l and l' label the unit cell. The force constants $\Phi_{\alpha\beta} \begin{pmatrix} l & l' \\ k & k' \end{pmatrix}$ obey the symmetry constraints [41]

$$\Phi(g\mathbf{L}) = \mathbf{S} \Phi(\mathbf{L}) \mathbf{S}^T, \quad (4)$$

where we have introduced the shorthand notation $\Phi_{\alpha\beta}(\mathbf{L}) \equiv \Phi_{\alpha\beta} \begin{pmatrix} l & l' \\ k & k' \end{pmatrix}$ with $\mathbf{L} \equiv \mathbf{r}(l') - \mathbf{r}(l)$, for the elements of the 3×3 matrix $\Phi(\mathbf{L})$. Here, $g \in P4mm$ denotes a space-group operation and $\mathbf{S} \in C_{4v}$ the corresponding 3×3 orthogonal matrix representation of the associated point-group operation [42]. In the present case, $\Phi(\mathbf{L})$ is nonzero only for the nearest-neighbor bonds \mathbf{L}_1 , \mathbf{L}_2 , \mathbf{L}_3 , and \mathbf{L}_4 shown in Fig. 2(a). To determine $\Phi(\mathbf{L}_1)$,

we identify the operations g satisfying $g\mathbf{L}_1 = \mathbf{L}_1$. The only symmetry elements that leave \mathbf{L}_1 invariant are E and σ_x . Consequently, $\Phi(\mathbf{L}_1) = \mathbf{S}_{\sigma_x} \Phi(\mathbf{L}_1) \mathbf{S}_{\sigma_x}^T$, from which we find the tensorial form

$$\Phi(\mathbf{L}_1) = - \begin{bmatrix} k_1 & 0 & k_4 \\ 0 & k_2 & 0 \\ k'_4 & 0 & k_3 \end{bmatrix}. \quad (5)$$

The remaining matrices $\Phi(\mathbf{L}_i)$ follow from successive fourfold rotations about the z -axis. Notably, the matrices are parametrized by five independent tensor coefficients: k_1, k_2, k_3, k_4 , and k'_4 . The resulting force constants are then used to construct the dynamical matrix via Eq. (3). For details, see the Supplemental Material (SM) [43].

We obtain analytic expressions by diagonalizing $\mathbf{D}(\mathbf{q})$ perturbatively to second order in \mathbf{q} near the Γ point with $m_1 = m_2 = m_3/2$ [43]. This low- \mathbf{q} expansion is particularly relevant as it captures the optically accessible Raman-active phonon modes near the Γ point. Below, we focus on the nondegenerate optical band [Fig. 2(b)]

$$\tilde{\omega}_2(\mathbf{q}) = \omega_0^{(2)} \sqrt{[1 - a^2 (q_x^2 + q_y^2) / 8]}, \quad (6)$$

with the following corresponding sublattice eigenvectors: $\mathbf{e}_2(1|\mathbf{q}) = [ia_x^{(2)}q_x, ia_y^{(2)}q_y, \sin\theta^{(2)}\cos\phi^{(2)}]$, $\mathbf{e}_2(2|\mathbf{q}) = [ib_x^{(2)}q_x, ib_y^{(2)}q_y, \sin\theta^{(2)}\sin\phi^{(2)}]$, $\mathbf{e}_2(3|\mathbf{q}) = [ic_x^{(2)}q_x, ic_y^{(2)}q_y, \cos\theta^{(2)}]$ [44]. Here, $\omega_0^{(2)} = \sqrt{4k_3/m_1}$, the parameters $a_i^{(2)}, b_i^{(2)}, c_i^{(2)}$ ($i = x, y, z$) depend on k_1, k_2, k_3, k_4, k'_4 and vanish in the limit $k_4, k'_4 \rightarrow 0$ [43], and the angles are given by $\theta^{(2)} = -\pi/4$, and $\phi^{(2)} = \pi/4$. The vector $\mathbf{e}_2(\mathbf{q})$ is normalized to order \mathbf{q} . The optical phonon (6) carry an angular momentum of the form $\mathbf{J} \propto \mathbf{q} \times \hat{\mathbf{z}}$ [43]. Since Γ is a time-reversal-invariant momentum, the angular momentum vanishes as $\mathbf{q} \rightarrow 0$.

The spin system is described by the Hamiltonian (A and B label the up and down spin lattice) [31–33]

$$H = H_1 + H_2 + H'_2 + H_a, \quad (7)$$

where $H_1 = J_1 \sum_{\langle i,j \rangle} \mathbf{S}_i^A \cdot \mathbf{S}_j^B$ denotes an antiferromagnetic exchange interaction with $J_1 > 0$, $H_2 = J_2 (\sum_{\langle i_x, j_x \rangle} \mathbf{S}_i^A \cdot \mathbf{S}_j^A + \sum_{\langle i_y, j_y \rangle} \mathbf{S}_i^B \cdot \mathbf{S}_j^B)$ and $H'_2 = J'_2 (\sum_{\langle i_y, j_y \rangle} \mathbf{S}_i^A \cdot \mathbf{S}_j^A + \sum_{\langle i_x, j_x \rangle} \mathbf{S}_i^B \cdot \mathbf{S}_j^B)$ represent ferromagnetic exchange interactions with $J_2, J'_2 < 0$, and $H_a = K_z \sum_i [(S_{i,z}^A)^2 + (S_{i,z}^B)^2]$ is an easy-axis anisotropy term with $K_z < 0$. $\langle i, j \rangle$, $\langle i_x, j_x \rangle$, and $\langle i_y, j_y \rangle$ denote nearest-neighbor bonds along the diagonal, x , and y directions, respectively. The collective spin excitations of Eq. (7) are obtained via a Holstein–Primakoff (HP) transformation [35], resulting in the bosonic Bogoliubov–de Gennes (BdG) Hamiltonian

$$H_m = \sum_{\mathbf{k}} \begin{pmatrix} a_{\mathbf{k}}^\dagger & b_{-\mathbf{k}} \end{pmatrix} \begin{pmatrix} A_{\mathbf{k}} & B_{\mathbf{k}} \\ B_{\mathbf{k}} & C_{\mathbf{k}} \end{pmatrix} \begin{pmatrix} a_{\mathbf{k}} \\ b_{-\mathbf{k}}^\dagger \end{pmatrix}. \quad (8)$$

Here, $A_{\mathbf{k}}, B_{\mathbf{k}}$, and $C_{\mathbf{k}}$ depend on J_1, J_2, J'_2 , and K_z (see SM [43]). To parameterize the altermagnetic splitting, we introduce $J_2 = \bar{J}_2 + \Delta J_2$ and $J'_2 = \bar{J}_2 - \Delta J_2$, such that $J_2 - J'_2 = 2\Delta J_2$. H_m is diagonalized by the BdG transformation $a_{\mathbf{k}} = u_{\mathbf{k}}\alpha_{\mathbf{k}} + v_{\mathbf{k}}\beta_{-\mathbf{k}}^\dagger$, $b_{-\mathbf{k}}^\dagger = v_{\mathbf{k}}^*\alpha_{\mathbf{k}} + u_{\mathbf{k}}^*\beta_{-\mathbf{k}}^\dagger$, which yields $H_m = \sum_{\mathbf{k}} [\omega_\alpha(\mathbf{k})\alpha_{\mathbf{k}}^\dagger\alpha_{\mathbf{k}} + \omega_\beta(\mathbf{k})\beta_{\mathbf{k}}^\dagger\beta_{\mathbf{k}}]$ with eigenenergies $\omega_\alpha(\mathbf{k}) = (A_{\mathbf{k}} - C_{\mathbf{k}} + \sqrt{(A_{\mathbf{k}} + C_{\mathbf{k}})^2 - 4B_{\mathbf{k}}^2})/2$, and $\omega_\beta(\mathbf{k}) = (C_{\mathbf{k}} - A_{\mathbf{k}} + \sqrt{(A_{\mathbf{k}} + C_{\mathbf{k}})^2 - 4B_{\mathbf{k}}^2})/2$. The resulting band splitting $\Delta\omega(\mathbf{k}) = \omega_\alpha(\mathbf{k}) - \omega_\beta(\mathbf{k})$ is shown in Fig. 2(c) and assumes the form

$$\Delta\omega(\mathbf{k}) = 4S\Delta J_2 [\cos(2k_x a) - \cos(2k_y a)]. \quad (9)$$

The characteristic d -wave symmetry is evident, yielding a finite spin splitting along the altermagnetic directions Γ -X and Γ -Y, and vanishing splitting along the symmetric direction Γ -M.

The magnon–phonon coupling originates from the modulation of the exchange interactions by lattice vibrations. To leading order in the atomic displacements, the exchange interaction between sites i and j becomes $J_{ij} = J_{ij}^0 + \alpha_{ij} \hat{\mathbf{n}}_{ij} \cdot \Delta\mathbf{u}_{ij}$, where J_{ij}^0 denotes the equilibrium exchange constant, $\alpha_{ij} = \partial J_{ij} / \partial a$ (a is the lattice constant) [45] is the spin–phonon coupling parameter, $\hat{\mathbf{n}}_{ij}$ is the unit vector pointing from site i to j , and $\Delta\mathbf{u}_{ij} = \mathbf{u}_j - \mathbf{u}_i$ with \mathbf{u}_i the displacement field of the atom at site i . Substituting this expansion into Eq. (7) yields the interaction Hamiltonian $H_I = H_{I1} + H_{I2} + H_{I3}$. The nearest-neighbor contribution reads $H_{I1} = \alpha_1 \sum_{\langle i,j \rangle} \hat{\mathbf{n}}_{ij} \cdot \Delta\mathbf{u}_{ij} \mathbf{S}_i^A \cdot \mathbf{S}_j^B$, with $\alpha_1 = \partial J_1 / \partial a$. The next-nearest-neighbor terms are $H_{I2} = \sum_{\langle i_x, j_x \rangle} \hat{\mathbf{n}}_{ij} \cdot \Delta\mathbf{u}_{ij} [\alpha_2 \mathbf{S}_i^A \cdot \mathbf{S}_j^A + \alpha'_2 \mathbf{S}_i^B \cdot \mathbf{S}_j^B]$ and $H_{I3} = \sum_{\langle i_y, j_y \rangle} \hat{\mathbf{n}}_{ij} \cdot \Delta\mathbf{u}_{ij} [\alpha_2 \mathbf{S}_i^B \cdot \mathbf{S}_j^B + \alpha'_2 \mathbf{S}_i^A \cdot \mathbf{S}_j^A]$ where $\alpha_2 \equiv \bar{\alpha}_2 + \Delta\alpha_2$ and $\alpha'_2 \equiv \bar{\alpha}_2 - \Delta\alpha_2$ are given by the derivatives of J_2 and J'_2 with respect to a . The displacement field at sublattice site k in unit cell l can be expanded in the phonon eigenmodes as [41] $\mathbf{u}(k, l) = \sqrt{1/Nm_k} \sum_{n,\mathbf{q}} \mathbf{e}_n(k|\mathbf{q}) Q_n(\mathbf{q}, t) \exp(i\mathbf{q} \cdot \mathbf{r}(k, l))$ where $Q_n(\mathbf{q}, t)$ denotes the normal coordinate and N the number of unit cells. Upon inserting this expansion together with the HP representation of the spin operators into H_I and performing a Fourier transformation to momentum space, we obtain the Hamiltonian [46]

$$H_I = \sum_{n,\mathbf{k},\mathbf{q}} [\Omega_{\bar{\alpha}\alpha}(n, \mathbf{q}, \mathbf{k}) \alpha_{\mathbf{k}+\mathbf{q}}^\dagger \alpha_{\mathbf{k}} + \Omega_{\bar{\beta}\beta}(n, \mathbf{q}, \mathbf{k}) \beta_{-\mathbf{k}}^\dagger \beta_{-\mathbf{k}-\mathbf{q}} + \Omega_{\bar{\alpha}\bar{\beta}}(n, \mathbf{q}, \mathbf{k}) \alpha_{\mathbf{k}+\mathbf{q}}^\dagger \beta_{-\mathbf{k}}^\dagger + \Omega_{\alpha\beta}(n, \mathbf{q}, \mathbf{k}) \alpha_{\mathbf{k}} \beta_{-\mathbf{k}-\mathbf{q}}] Q_n(\mathbf{q}, t), \quad (10)$$

where the coupling vertices Ω are given in the SM [43].

Next, we examine the generation of altermagnonic dc spin currents driven by selective phonon excitations in the stationary regime. The nonequilibrium correction to the magnon distribution function $n_\gamma(\mathbf{k}) = \langle \gamma_{\mathbf{k}}^\dagger(t) \gamma_{\mathbf{k}}(t) \rangle$ arising from the coupling to an excited phonon mode

(n, \mathbf{q}) can be expressed in terms of the magnons' Keldysh Green's function $G_{\gamma\bar{\gamma}}^K(\mathbf{k}; \omega)$ as [47]

$$\Delta n_\gamma(\mathbf{k}) = \frac{i}{4\pi} \int_{-\infty}^{\infty} G_{\gamma\bar{\gamma}}^K(\mathbf{k}; \omega) d\omega, \quad (11)$$

where $\gamma \in \{\alpha, \beta\}$. G^K is obtained from the contour-ordered Green's function $G_{\gamma\bar{\gamma}}^{(\tau\tau')}(\mathbf{k}, t; \mathbf{k}', t') = -i\langle \mathcal{T}_c e^{-\frac{i}{\hbar} \int_c H_I(t_1) dt_1} \gamma_{\mathbf{k}}(t, \tau) \gamma_{\mathbf{k}'}^\dagger(t', \tau') \rangle_0$, where the subscript 0 denotes averaging over the equilibrium state in the infinite past, in which the system is noninteracting. The operator \mathcal{T}_c enforces time ordering along the Keldysh contour c , whose upper/lower branch is labeled by τ and τ' . All operators are taken in the interaction picture. The interaction Hamiltonian H_I includes the contribution from a single phonon mode (n, \mathbf{q}) , corresponding to a normal coordinate of the form [41] $Q_{n'}(\mathbf{q}', t) = (A_n(\mathbf{q})/2)\delta_{nn'}\delta_{\mathbf{q}, \mathbf{q}'} e^{-i\tilde{\omega}_n(\mathbf{q})t} + (A_n^*(\mathbf{q})/2)\delta_{nn'}\delta_{-\mathbf{q}, \mathbf{q}'} e^{i\tilde{\omega}_n(\mathbf{q})t}$, where $A_n(\mathbf{q})$ parametrizes the oscillation amplitude. We evaluate $G_{\gamma\bar{\gamma}}^{(\tau\tau')}$ to second order in the magnon-phonon interaction. Expanding $G_{\gamma\bar{\gamma}}^{(\tau\tau')}$ to second order in H_I , applying Wick's theorem, and transforming to frequency space and the triangular representation in Keldysh space, we find the equation

$$\underline{G}_{\gamma\bar{\gamma}}(\mathbf{k}; \omega) = \underline{G}_{\gamma\bar{\gamma}}(\mathbf{k}; \omega)_0 + \underline{G}_{\gamma\bar{\gamma}}(\mathbf{k}; \omega)_0 \underline{\Sigma}_{\gamma\bar{\gamma}}(\mathbf{k}; \omega) \underline{G}_{\gamma\bar{\gamma}}(\mathbf{k}; \omega)_0, \quad (12)$$

with $\underline{G} = [G^R, G^K; 0, G^A]$ and $\underline{\Sigma} = [\Sigma^R, \Sigma^K; 0, \Sigma^A]$. Here, $G^{R(A)}$ denotes the retarded (advanced) Green's function, and the self-energy $\underline{\Sigma}$ is evaluated to second order in H_I (see SM [43]). Extracting the Keldysh component of Eq. (12) and substituting it into Eq. (11), we obtain the following nonequilibrium correction to the magnon distribution function [43]

$$\Delta n_\gamma(\mathbf{k}, \mathbf{q}) = \sum_{\eta=\pm 1} \left[\frac{K_{1\gamma}(n, \eta\mathbf{q}, \mathbf{k})(2n_\gamma^0(\mathbf{k} + \eta\mathbf{q}) + 1)}{(\omega_\gamma(\mathbf{k} + \eta\mathbf{q}) - \omega_\gamma(\mathbf{k}) - \eta\tilde{\omega}_n(\mathbf{q}))^2 + \varepsilon^2} + \frac{K_{2\gamma}(n, \eta\mathbf{q}, \mathbf{k})(2n_\gamma^0(-\mathbf{k} - \eta\mathbf{q}) + 1)}{(\omega_\gamma(-\mathbf{k} - \eta\mathbf{q}) + \omega_\gamma(\mathbf{k}) + \eta\tilde{\omega}_n(\mathbf{q}))^2 + \varepsilon^2} \right], \quad (13)$$

where $\underline{\alpha} = \beta, \underline{\beta} = \alpha$, and $n_\gamma^0(\mathbf{k})$ is the Bose-Einstein distribution. The coefficients $K_{1\gamma}$ and $K_{2\gamma}$ depend on the coupling vertices Ω in Eq. (10) and can be found in the SM [43]. Additionally, we have included a phenomenological damping rate ε , approximated as $\varepsilon = \alpha_G \omega_\gamma(0)$ where α_G is the Gilbert damping parameter.

Eq. (13) allows us to identify the dominant processes contributing to the nonequilibrium distribution function. The first term describes single-magnon processes in which a magnon γ either absorbs or emits a phonon with momentum \mathbf{q} and energy $\tilde{\omega}_n(\mathbf{q})$. Energy conservation requires $\omega_\gamma(\mathbf{k} + \mathbf{q}) = \omega_\gamma(\mathbf{k}) + \tilde{\omega}_n(\mathbf{q})$ for absorption and $\omega_\gamma(\mathbf{k} - \mathbf{q}) = \omega_\gamma(\mathbf{k}) - \tilde{\omega}_n(\mathbf{q})$ for emission. The second term describes two-magnon processes in which magnons

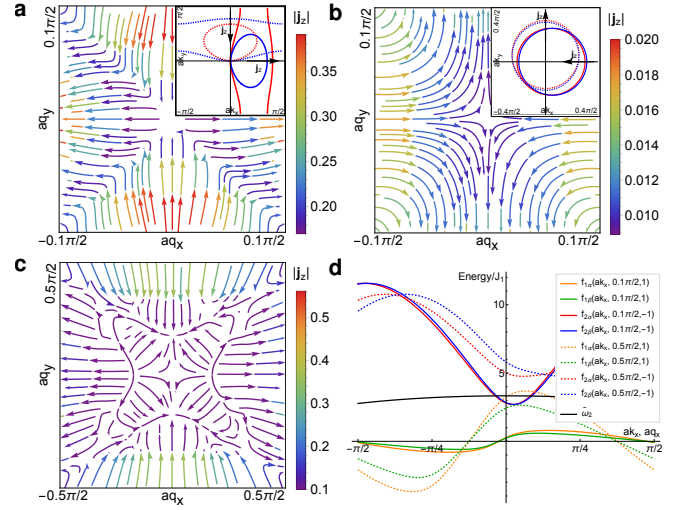


FIG. 3. Dimensionless spin current $\mathbf{j}^z(\mathbf{q}) = (4\pi^2 a/J_1) \mathbf{J}^z(\mathbf{q})$ as a function of the phonon momentum \mathbf{q} for three phonon spectra $\tilde{\omega}_2(\mathbf{q}) = \omega_0^{(2)} \sqrt{1 - a^2(q_x^2 + q_y^2)}/8$: (a) $\omega_0^{(2)} = 0.1\omega_0$, (b) $\omega_0^{(2)} = 2.0\omega_0$, and (c) $\omega_0^{(2)} = 1.3\omega_0$, where $\omega_0 = 4S\sqrt{K_z^2 - 4J_1 K_z}$. The insets in (a) and (b) show the resonant \mathbf{k} states governing the induced spin current. (d) Functions $f_{1\gamma}$ and $f_{2\gamma}$ versus ak_x for $a\mathbf{q} = 0.1\pi\hat{x}/2$ (solid lines) and $a\mathbf{q} = 0.5\pi\hat{x}/2$ (dotted lines), together with $\tilde{\omega}_2(\mathbf{q})$ for $\omega_0^{(2)} = 1.3\omega_0$. In all calculations, we use $J_1 = 25.7$ meV, $K_z/J_1 = -0.1$, $\bar{J}_2/J_1 = -0.4$, $\Delta J_2/J_1 = -0.2$, $\alpha_1 = -53$ meV/Å, $\bar{\alpha}_2/\alpha_1 = -0.4$, $\Delta\alpha_2/\alpha_1 = -0.2$, $\alpha_G = 10^{-1}$, $\sqrt{A_n^2/(Nm_1 a^2)} = 10^{-2}$, $T = 298$ K, $\hbar = S = 1$, and $a = 4$ Å.

γ and $\bar{\gamma}$ are either created (annihilated) accompanied by phonon annihilation (creation). For small \mathbf{q} , one has $\omega_\gamma(\mathbf{k} + \eta\mathbf{q}) \approx \omega_\gamma(\mathbf{k})$, implying that the single-magnon processes are resonant at small phonon energies. In contrast, the two-magnon processes require a comparatively large phonon energy due to the conservation of the energy of both magnons. Consequently, the second term in Eq. (13) dominates at higher phonon energies. Importantly, as shown below, *these two mechanisms generate phonon-driven magnon spin currents of opposite sign, enabling a reversal of the spin current by tuning the frequency of the excited phonon.*

The spin current polarized along z and flowing in the direction $i \in \{x, y\}$ is calculated from the expression

$$J_i^z(\mathbf{q}) = \frac{\hbar}{A} \sum_{\mathbf{k}} \left[v_i^\alpha(\mathbf{k}) \Delta n_\alpha(\mathbf{k}, \mathbf{q}) - v_i^\beta(\mathbf{k}) \Delta n_\beta(\mathbf{k}, \mathbf{q}) \right]. \quad (14)$$

Here, A denotes the area of the sample and $v_i^\gamma(\mathbf{k}) = \partial\omega_\gamma(\mathbf{k})/\partial k_i$ is the group velocity. The summation runs over all \mathbf{k} values within the first Brillouin zone (FBZ).

Figs. 3(a)-(b) show the spin current generated by the $n = 2$ phonon mode in Eq. (6) as a function of \mathbf{q} for $\omega_0^{(2)} = 0.1\omega_0$ and $\omega_0^{(2)} = 2.0\omega_0$, respectively. Here, $\omega_0 = 4S\sqrt{K_z^2 - 4J_1 K_z}$. In both cases, the resulting spin current is strongly anisotropic and exhibits a pronounced

d -wave symmetry, consistent with the anisotropic thermally driven magnon spin current reported in Ref. [24]. A key observation is the sign reversal of the spin current along the altermagnetic directions $[\pm 1, 0, 0]$ and $[0, \pm 1, 0]$ when $\omega_0^{(2)}$ is changed from $0.1\omega_0$ to $2.0\omega_0$. This behavior can be understood by analyzing the dominant \mathbf{k} states contributing to the spin current (14). These correspond to $\mathbf{k} \in \text{FBZ}$ satisfying one of the resonance conditions $f_{1\gamma}(\mathbf{k}, \mathbf{q}, \eta) = \tilde{\omega}_2(\mathbf{q})$ or $f_{2\gamma}(\mathbf{k}, \mathbf{q}, \eta) = \tilde{\omega}_2(\mathbf{q})$, where $f_{1\gamma} \equiv \omega_\gamma(\mathbf{k} + \eta\mathbf{q}) - \omega_\gamma(\mathbf{k})$ and $f_{2\gamma} \equiv \omega_\gamma(-\mathbf{k} - \eta\mathbf{q}) + \omega_\gamma(\mathbf{k})$ define the resonance conditions for single-magnon and two-magnon processes, respectively. For $\omega_0^{(2)} = 0.1\omega_0$, single-magnon processes dominate; i.e., there exist $\mathbf{k} \in \text{FBZ}$ satisfying $f_{1\gamma}(\mathbf{k}, \mathbf{q}, \eta) = \tilde{\omega}_2(\mathbf{q})$. The corresponding resonant \mathbf{k} states are shown in the inset of Fig. 3(a) for $\mathbf{q} = (0.1\pi/2a)\hat{\mathbf{x}}$ (solid lines) and $\mathbf{q} = (0.1\pi/2a)\hat{\mathbf{y}}$ (dotted lines) with $\eta = +1$. The case $\eta = -1$ yields a similar distribution, shifted slightly along \mathbf{q} . For \mathbf{q} along x , the sum in Eq. (14) receives a larger contribution from α -magnon \mathbf{k} -states (red lines) carrying spin $+\hbar$ and velocity $v_x^\alpha > 0$ than from the corresponding β -magnon states (blue lines), resulting in a positive spin current along x . For \mathbf{q} along y , the dominant contribution arises from β -magnons (blue lines) with spin $-\hbar$ and velocity $v_y^\beta > 0$, producing a negative spin current along y . For $\omega_0^{(2)} = 2.0\omega_0$, the resonant processes are two-magnon processes, with the corresponding dominant \mathbf{k} states shown in the inset of Fig. 3(b). In this regime, β -magnons with $v_x^\beta > 0$ dominate for \mathbf{q} along x , resulting in a negative spin current along this direction, while the situation is reversed for \mathbf{q} along y . Since the resonant α and β states are only weakly shifted in momentum space for the two-magnon processes compared with the single-magnon case [inset of Fig. 3(b) versus Fig. 3(a)], the resulting spin current is smaller.

The picture becomes more intricate when $\omega_0^{(2)}$ approaches ω_0 , corresponding to the lower bound of $f_{2\gamma}$. In this regime, the resonant magnon states satisfy either $f_{1\gamma}(\mathbf{k}, \mathbf{q}, \eta) = \tilde{\omega}_2(\mathbf{q})$ or $f_{2\gamma}(\mathbf{k}, \mathbf{q}, \eta) = \tilde{\omega}_2(\mathbf{q})$, depending on the magnitude of $|\mathbf{q}|$. This is illustrated in Fig. 3(d), which shows $f_{1\gamma}$ and $f_{2\gamma}$ as functions of ak_x for $a\mathbf{q} = 0.1\pi/2\hat{\mathbf{x}}$ (solid lines) and $a\mathbf{q} = 0.5\pi/2\hat{\mathbf{x}}$ (dotted lines), together with the phonon energy $\tilde{\omega}_2(\mathbf{q})$ for $\omega_0^{(2)} = 1.3\omega_0$. As $|\mathbf{q}|$ increases for a fixed direction of \mathbf{q} , the resonant processes switch from two-magnon to single-magnon character, as shown in Fig. 3(c). Consequently, reversing $J_i^z(\mathbf{q})$ does not require a full inversion of \mathbf{q} ; a modest change in the excitation frequency is sufficient.

Both the d -wave symmetry of the phonon-induced spin current and its sign reversal upon tuning the excitation frequency constitute symmetry-governed fingerprints of altermagnetism in magnon transport. Both effects originate from the momentum-dependent chiral band splitting and vanish in the limit $\Delta J_2 \rightarrow 0$. Our results therefore demonstrate that altermagnets provide a unique platform

for tunable spin transport, where altermagnonic spin currents can be controlled through both the frequency and the momentum of selectively excited phonons.

KMDH acknowledges funding from the Research Council of Norway via Project No. 334202. MK acknowledges support from the Research Council of Norway through its Centers of Excellence funding scheme, Project No. 262633 "QuSpin".

-
- [1] L. Šmejkal, J. Sinova, and T. Jungwirth, Beyond Conventional Ferromagnetism and Antiferromagnetism: A Phase with Nonrelativistic Spin and Crystal Rotation Symmetry," Phys. Rev. X **12**, 031042 (2022).
 - [2] L. Šmejkal, J. Sinova, and T. Jungwirth, Emerging Research Landscape of Altermagnetism, Phys. Rev. X **12**, 040501 (2022).
 - [3] J. Krempaský, L. Šmejkal, S. W. D'Souza, M. Hajlaoui, G. Springholz, K. Uhlířová, F. Alarab, P. C. Constantinou, V. Strocov, D. Usanov, W. R. Pudelko, R. González-Hernández, A. Birk Hellenes, Z. Jansa, H. Reichlová, Z. Šobán, R. D. Gonzalez Betancourt, P. Wadley, J. Sinova, D. Kriegner, J. Minár, J. H. Dil, and T. Jungwirth, Altermagnetic lifting of Kramers spin degeneracy, Nature **626**, 517 (2024).
 - [4] S. Lee, S. Lee, S. Jung, J. Jung, D. Kim, Y. Lee, B. Seok, J. Kim, B. G. Park, L. Šmejkal, C.-J. Kang, and C. Kim, Broken Kramers Degeneracy in Altermagnetic MnTe, Phys. Rev. Lett. **132**, 036702 (2024).
 - [5] Osumi, T. Osumi, S. Souma, T. Aoyama, K. Yamauchi, A. Honma, K. Nakayama, T. Takahashi, K. Ohgushi, and T. Sato, Observation of a giant band splitting in altermagnetic MnTe, Phys. Rev. B **109**, 115102 (2024).
 - [6] M. Hajlaoui, S. W. D'Souza, L. Šmejkal, D. Kriegner, G. Krizman, T. Zakusylo, N. Olszowska, O. Caha, J. Michalička, J. Sánchez-Barriga, A. Marmodoro, K. Výborný, A. Ernst, M. Cinchetti, J. Minar, T. Jungwirth, G. Springholz, Temperature Dependence of Relativistic Valence Band Splitting Induced by an Altermagnetic Phase Transition, Advanced Materials **36**, 2314076 (2024).
 - [7] S. Reimers, L. Odenbreit, L. Šmejkal, V. N. Strocov, P. Constantinou, A. B. Hellenes, R. Jaeschke Ubiergo, W. H. Campos, V. K. Bharadwaj, A. Chakraborty, T. Deneulin, W. Shi, R. E. Dumin-Borkowski, S. Das, M. Kläui, J. Sinova, and Martin Jourdan, Direct observation of altermagnetic band splitting in CrSb thin films, Nature Communications **15**, 2116 (2024).
 - [8] J. Liu, Y. Yang, R. Zhang, L. Deng, W. Jing, Y. Huang, Y. Shi, M. Ye, S. Qiao, Y. Wang, Y. Guo, D. Feng, and D. Shen, Large Band Splitting in g-Wave Altermagnet CrSb, Phys. Rev. Lett. **133**, 206401 (2024).
 - [9] M. Zeng, M.-Y. Zhu, Y.-P. Zhu, X.-R. Liu, X.-M. Ma, Y.-J. Hao, P. Liu, G. Qu, Y. Yang, Z. Jiang, K. Yamagami, M. Arita, X. Zhang, T.-H. Shao, Y. Dai, K. Shimada, Z. Liu, M. Ye, Y. Huang, Q. Liu, and C. Liu, Observation of Spin Splitting in Room-Temperature Metallic Antiferromagnet CrSb, Advanced Science **11**, 2406529 (2024).
 - [10] G. Yang, Z. Li, S. Yang, J. Li, H. Zheng, W. Zhu, Z. Pan, Y. Xu, S. Cao, W. Zhao, A. Jana, J. Zhang, M.

- Ye, Y. Song, L.-H. Hu, L. Yang, J. Fujii, I. Vobornik, M. Shi, H. Yuan, Y. Zhang, Y. Xu, and Y. Liu, Three-dimensional mapping of the altermagnetic spin splitting in CrSb, *Nature Communications* **16**, 1442 (2025).
- [11] C. Li, M. Hu, Z. Li, Y. Wang, W. Chen, B. Thiagarajan, M. Leandersson, C. Polley, T. Kim, H. Liu, C. Fulga, M. G. Vergniory, O. Janson, O. Tjernberg, and J. van den Brink, *Topological Weyl Altermagnetism in CrSb*, *Communications Physics* **8**, 311 (2025).
- [12] W. Lu, S. Feng, Y. Wang, D. Chen, Z. Lin, X. Liang, S. Liu, W. Feng, K. Yamagami, J. Liu, C. Felser, Q. Wu, and J. Ma, Observation of surface Fermi arcs in altermagnetic Weyl semimetal CrSb, *Nano Lett.* **25**, 7343 (2025).
- [13] B. Jiang, M. Hu, J. Bai, Z. Song, C. Mu, G. Qu, W. Li, W. Zhu, H. Pi, Z. Wei, Y.-J. Sun, Y. Huang, X. Zheng, Y. Peng, L. He, S. Li, J. Luo, Z. Li, G. Chen, H. Li, H. Weng, and T. Qian, A metallic room-temperature d-wave altermagnet, *Nature Physics* **21**, 754 (2025).
- [14] F. Zhang, X. Cheng, Z. Yin, C. Liu, L. Deng, Y. Qiao, Z. Shi, S. Zhang, J. Lin, Z. Liu, M. Ye, Y. Huang, X. Meng, C. Zhang, T. Okuda, K. Shimada, S. Cui, Y. Zhao, G.-H. Cao, S. Qiao, J. Liu, and C. Chen, Crystal-symmetry-paired spin-valley locking in a layered room-temperature metallic altermagnet candidate. *Nature Physics* **21**, 760 (2025).
- [15] T. Jungwirth, J. Sinova, P. Wadley, D. Kriegner, H. Reichlova, F. Krizek, H. Ohno, L. Šmejkal, *Altermagnetic spintronics*, arXiv:2508.09748.
- [16] Z. Feng, X. Zhou, L. Šmejkal, L. Wu, Z. Zhu, H. Guo, R. González-Hernández, X. Wang, H. Yan, P. Qin, X. Zhang, H. Wu, H. Chen, Z. Xia, C. Jiang, M. Coey, J. Sinova, T. Jungwirth, and Z. Liu, An anomalous Hall effect in altermagnetic ruthenium dioxide, *Nat. Electron.* **5**, 735 (2022).
- [17] S. Das, A. Ross, X. X. Ma, S. Becker, C. Schmitt, F. van Duijn, E. F. Galindez-Ruales, F. Fuhrmann, M.-A. Syskaki, U. Ebels, V. Baltz, A.-L. Barra, H. Y. Chen, G. Jakob, S. X. Cao, J. Sinova, O. Gomonay, R. Lebrun, and M. Kläui, Anisotropic long-range spin transport in canted antiferromagnetic orthoferrite YFeO₃, *Nature Communications* **13**, 6140 (2022).
- [18] R. D. Gonzalez Betancourt, J. Zubáč, R. Gonzalez-Hernandez, K. Geishendorf, Z. Šobán, G. Springholz, K. Olejník, L. Šmejkal, J. Sinova, T. Jungwirth, S. T. B. Goennenwein, A. Thomas, H. Reichlová, J. Železný, and D. Kriegner, Spontaneous anomalous Hall effect arising from an unconventional compensated magnetic phase in a semiconductor, *Phys. Rev. Lett.* **130**, 036702 (2023).
- [19] L. Han, X. Z. Fu, R. Peng, X. K. Cheng, J. K. Dai, L. Y. Liu, Y. D. Li, Y. C. Zhang, W. X. Zhu, H. Bai, Y. J. Zhou, S. X. Liang, C. Chen, Q. Wang, X. Z. Chen, L. Y. Yang, Y. Zhang, C. Song, J. W. Liu, and F. Pan, Electrical 180° switching of Néel vector in spin-splitting antiferromagnet, *Sci. Adv.* **10**, eadn0479 (2024).
- [20] R. Y. Chu, L. Han, Z. H. Gong, X. Z. Fu, H. Bai, S. X. Liang, C. Chen, S.-W. Cheong, Y. Y. Zhang, J. W. Liu, Y. Y. Wang, F. Pan, H. Z. Lu, and C. Song, Third-Order Nonlinear Hall Effect in Altermagnet RuO₂, *Phys. Rev. Lett.* **135**, 216703 (2025).
- [21] A. Badura, W. H. Campos, V. K. Bharadwaj, I. Kounta, L. Michez, M. Petit, Javier Rial, M. Leiviskä, V. Baltz, F. Krizek, D. Kriegner, J. Železný, J. Zemen, S. Telkamp, S. Sailler, M. Lammel, R. Jaeschke-Ubiergo, A. B. Hellenes, R. González-Hernández, J. Sinova, T. Jungwirth, S. T. B. Goennenwein, L. Šmejkal, and H. Reichlova, Observation of the anomalous Nernst effect in altermagnetic candidate Mn₅Si₃, *Nature Communications* **16**, 7111 (2025).
- [22] Z. Y. Zhou, X. K. Cheng, M. L. Hu, R. Y. Chu, H. Bai, L. Han, J. W. Liu, F. Pan, and C. Song, Manipulation of the altermagnetic order in CrSb via crystal symmetry, *Nature (London)* **638**, 645 (2025).
- [23] L. Han, X. Z. Fu, W. Q. He, J. K. Dai, Y. X. Zhu, W. F. Yang, Y. L. Chen, J. C. Zhang, W. X. Zhu, H. Bai, C. Chen, D. Z. Hou, C. H. Wan, X. F. Han, C. Song, J. W. Liu, and F. Pan, Nonvolatile anomalous Nernst effect in Mn₅Si₃ with a collinear Néel vector, *Phys. Rev. Appl.* **23**, 044066 (2025).
- [24] E. Galindez-Ruales, W. Yang, T. Danegger, M. Kundu, Jonas Köhler, C. Schmitt, F. Fuhrmann, A. Akashdeep, D. Minh Tran, X. Ma, G. Jakob, S. Cao, U. Nowak, and M. Kläui, Altermagnetic magnon transport in the d-wave altermagnet LuFeO₃, arXiv:2508.14569.
- [25] E. Galindez-Ruales, R. Gonzalez-Hernandez, C. Schmitt, S. Das, F. Fuhrmann, A. Ross, E. Golias, A. Akashdeep, L. Lünenbürger, E. Baek, W. Yang, L. Šmejkal, V. Krishna, R. Jaeschke-Ubiergo, J. Sinova, A. Rothschild, C.-Y. You, G. Jakob, and M. Kläui, Revealing the altermagnetism in hematite via XMCD imaging and anomalous Hall electrical transport, *Adv. Mater.* **37**, e05019 (2025).
- [26] O. J. Amin, A. Dal Din, E. Golias, Y. Niu, A. Zakharov, S. C. Fromage, C. J. B. Fields, S. L. Heywood, R. B. Cousins, F. Maccherozzi, J. Krempaský, J. H. Dil, D. Kriegner, B. Kiraly, R. P. Champion, A. W. Rushforth, K. W. Edmonds, S. S. Dhesi, L. Šmejkal, T. Jungwirth, and P. Wadley, Nanoscale imaging and control of altermagnetism in MnTe, *Nature* **636**, 348 (2024).
- [27] H. Pan, R.-C. Xiao, J. Han, H. Zhu, J. Li, Qian Niu, Y. Gao, and D. Hou, Experimental Evidence of Néel-Order-Driven Magneto-optical Kerr Effect in an Altermagnetic Insulator, *Phys. Rev. Lett.* **136**, 036701 (2026).
- [28] H. Bai, L. Han, X. Y. Feng, Y. J. Zhou, R. X. Su, Q. Wang, L. Y. Liao, W. X. Zhu, X. Z. Chen, F. Pan, X. L. Fan, and C. Song, Observation of Spin Splitting Torque in a Collinear Antiferromagnet RuO₂, *Phys. Rev. Lett.* **128**, 197202 (2022).
- [29] S. Karube, T. Tanaka, D. Sugawara, N. Kadoguchi, M. Kohda, and J. Nitta, Observation of Spin-Splitter Torque in Collinear Antiferromagnetic RuO₂, *Phys. Rev. Lett.* **129**, 137201 (2022).
- [30] A. Bose, N. J. Schreiber, R. Jain, D.-F. Shao, H. P. Nair, J. Sun, X. S. Zhang, D. A. Muller, E. Y. Tsybal, D. G. Schlom, and D. C. Ralph, Tilted spin current generated by the collinear antiferromagnet ruthenium dioxide, *Nature Electronics* **5**, 267 (2022).
- [31] L. Šmejkal, A. Marmodoro, K.-H. Ahn, R. González-Hernández, I. Turek, S. Mankovsky, H. Ebert, S. W. D'Souza, O. Šipr, J. Sinova, and T. Jungwirth, Chiral Magnons in Altermagnetic RuO₂, *Phys. Rev. Lett.* **131**, 256703 (2023).
- [32] B. Brekke, A. Brataas, and A. Sudbø, Two-dimensional altermagnets: Superconductivity in a minimal microscopic model, *Phys. Rev. B* **108**, 224421 (2023).
- [33] Q. Cui, B. Zeng, P. Cui, T. Yu, and H. Yang, Efficient spin Seebeck and spin Nernst effects of magnons in altermagnets, *Phys Rev B* **108**, L180401 (2023).
- [34] O. Gomonay, V. P. Kravchuk, R. Jaeschke-Ubiergo, K. V. Yershov, T. Jungwirth, L. Šmejkal, J. van den Brink,

- and J. Sinova, Structure, control, and dynamics of altermagnetic textures, NPJ Spintronics 2:35 (2024).
- [35] A. Auerbach, *Interacting Electrons and Quantum Magnetism* (Springer-Verlag, New York, 1994).
- [36] Z. Liu, M. Ozeki, S. Asai, S. Itoh, and T. Masuda, Chiral split magnon in altermagnetic MnTe, Phys. Rev. Lett. **133**, 156702 (2024).
- [37] Q. Sun, J. Guo, D. Wang, D. L. Abernathy, W. Tian, and C. Li, Observation of Chiral Magnon Band Splitting in Altermagnetic Hematite, Phys. Rev. Lett. **135**, 186703 (2025).
- [38] H. Bending, A. Mook, I. Mertig, and R. R. Neumann, D-Wave Phonon Angular Momentum Texture in Altermagnets by Magnon-Phonon-Hybridization, arXiv:2511.08357.
- [39] W. Jiang, S. Zhang, Z. Wang, F. Liu, and T. Low, Topological Band Engineering of Lieb Lattice in Phthalocyanine-Based Metal-Organic Frameworks, Nano Letters **20**, 1959 (2020).
- [40] M. R. Slot, T. S. Gardenier, P. H. Jacobse, G. C. P. van Miert, S. N. Kempkes, S. J. M. Zevenhuizen, C. M. Smith, D. Vanmaekelbergh, and I. Swart, Experimental realization and characterization of an electronic Lieb lattice, Nature Physics **13**, 672 (2017).
- [41] P. Brüesch, *Phonons: Theory and Experiments I: Lattice Dynamics and Models of Interatomic Forces*, Springer Series in Solid-State Sciences, Vol. 34 (Springer-Verlag, Berlin Heidelberg, 1982).
- [42] In the absence of SOC, the phonon system is independent of the spin configuration, causing the time reversal operator \mathcal{T} in the magnetic plane point group to be irrelevant. Consequently, in Eq. (4), $\mathbf{S} \in \{E, C_{2z}, \sigma_x, \sigma_y, C_{4z}^+, C_{4z}^-, \sigma_{xy}, \sigma_{x\bar{y}}\}$.
- [43] See the Supplemental Material (SM) for details of the derivation of the phonon and magnon models, the magnon–phonon coupling, and the phonon-induced magnon excitations. The SM includes Refs. [35, 41, 47, 48].
- [44] The remaining five optical modes form two doubly degenerate bands and a nondegenerate band at Γ [43].
- [45] For simplicity, we assume radially isotropic exchange parameters, which provide a good microscopic approximation for direct-exchange magnets with quenched orbital degrees of freedom.
- [46] Note that the phonon angular momentum $\mathbf{J} \propto \mathbf{q} \times \hat{\mathbf{z}}$ does not enter H_I explicitly. The coupling is governed by the projections $\hat{\mathbf{n}}_{ij} \cdot \Delta \mathbf{u}_{ij}$, which are insensitive to circular atomic motion in planes containing $\hat{\mathbf{z}}$ because $\hat{\mathbf{n}}_{ij} \cdot \hat{\mathbf{z}} = 0$. Consequently, rotational components of the lattice displacements do not couple directly to the magnon sector.
- [47] J. Rammer, *Quantum Field Theory of Non-Equilibrium States* (Cambridge University Press, Cambridge, 2007).
- [48] H. Haug and A. P. Jauho, *Quantum Kinetics in Transport and Optics of Semiconductors*, Springer-Verlag Berlin Heidelberg (2008).
- [49] S. H. Ursin, M. Kläui, and K. M. D. Hals, *Replication Data for: Tunable Phonon-Driven Magnon Spin Currents in Altermagnets*, DataverseNO, V1 (2026); DOI to be provided.